

1 **High-level cognition is supported by information-rich but**
2 **compressible brain activity patterns**

3 Lucy L. W. Owen^{1,2} and Jeremy R. Manning^{1,*}

1 Department of Psychological and Brain Sciences,
Dartmouth College, Hanover, NH

2 Carney Institute for Brain Sciences,
Brown University, Providence, RI

*Address correspondence to jeremy.r.manning@dartmouth.edu

4 December 22, 2023

5 **Abstract**

6 Brain activity patterns are highly flexible and often complex, but also highly structured.
7 Here we examined how fundamental properties of brain activity patterns relate to ongoing
8 cognitive processes. To this end, we applied dimensionality reduction algorithms and pattern
9 classifiers to functional neuroimaging data collected as participants listened to a story, tem-
10 porally scrambled versions of the story, or underwent a resting state scanning session. These
11 experimental conditions were intended to require different depths of processing and inspire
12 different levels of cognitive engagement. We considered two primary aspects of the data. First,
13 we treated the maximum achievable decoding accuracy across participants as an indicator of
14 the “informativeness” of the recorded patterns. Second, we treated the number of features
15 (components) required to achieve a threshold decoding accuracy as a proxy for the “compress-
16 ability” of the neural patterns (where fewer components indicate greater compression). Overall,
17 we found that the peak decoding accuracy (achievable without restricting the numbers of fea-
18 tures) was highest in the intact (unscrambled) story listening condition. However, the number
19 of features required to achieve comparable classification accuracy was also lowest in the intact
20 story listening condition. Taken together, our work suggests that our brain networks flexibly
21 reconfigure according to ongoing task demands, and that the activity patterns associated with
22 higher-order cognition and high engagement are both more informative and more compressible
23 than the activity patterns associated with lower-order tasks and lower levels of engagement.

24 **Keywords:** information, compression, temporal decoding, dimensionality reduction, neu-
25 roimaging

26 **Significance Statement:** How our brains respond to ongoing experiences depends on what
27 we are doing and thinking about, how engaged we are, and our past experiences, among other
28 factors. To gain insights into how brain activity patterns reflect ongoing cognitive processes, we
29 examined two fundamental aspects of brain activity under different cognitive circumstances:
30 informativeness and compressibility. Informativeness refers to the extent to which brain pat-
31 terns are both temporally specific and consistent across different people. Compressibility refers
32 to the extent to how robust the informativeness of brain patterns is to dimensionality reduction.
33 We found that brain activity patterns evoked by higher-level cognitive tasks are both more
34 informative *and* more compressible than activity evoked by lower-level tasks. Our findings
35 suggest that our brains flexibly reconfigure themselves to optimize different aspects of how
36 they function according to ongoing cognitive demands.

37 Introduction

38 Large-scale networks, including the human brain, may be conceptualized as occupying one or
39 more positions along on a continuum. At one extreme, every node is fully independent from
40 every other node. At the other extreme, all nodes behave identically. Each extreme optimizes
41 key properties of how the network functions. When every node is independent, the network is
42 maximally *expressive*: if we define the network's "state" as the activity pattern across its nodes, then
43 every state is equally reachable by a network with fully independent nodes. On the other hand, a
44 network of identically behaved nodes optimizes *robustness*: any subset of nodes may be removed
45 from the network without any loss of function or expressive power, as long as any single node
46 remains. Presumably, most natural systems tend to occupy positions between these extremes. We
47 wondered: might the human brain reconfigure itself to be more flexible or more robust according
48 to ongoing demands? In other words, might the brain reconfigure its connections or behaviors
49 under different circumstances to change its position along this continuum?

50 Closely related to the above notions of expressiveness versus robustness are measures of
51 how much *information* is contained in a given signal or pattern, and how *redundant* a signal
52 is (Shannon, 1948). Formally, information is defined as the amount of uncertainty about a given
53 variables' outcomes (i.e., entropy), measured in *bits*, or the optimal number of yes/no questions
54 needed to reduce uncertainty about the variable's outcomes to zero. Highly complex systems with
55 many degrees of freedom (i.e., high flexibility and expressiveness), are more information-rich than
56 simpler or more constrained systems. The redundancy of a signal denotes the difference between
57 how expressive the signal *could* be (i.e., proportional to the number of unique states or symbols
58 used to transmit the signal) and the actual information rate (i.e., the entropy of each individual
59 state or symbol). If a brain network's nodes are fully independent, then the number of bits required
60 to express a single activity pattern is proportional to the number of nodes. The network would
61 also be minimally redundant, since the status of every node would be needed to fully express a
62 single brain activity pattern. If a brain network's nodes are fully coupled and identical, then the
63 number of bits required to express a single activity pattern is proportional to the number of unique
64 states or values any individual node can take on. Such a network would be highly redundant,
65 since knowing any individual node's state would be sufficient to recover the full-brain activity

66 pattern. Highly redundant systems are also robust, since there is little total information loss due
67 to removing any given observation.

68 We take as a given that brain activity is highly flexible: our brains can exhibit nearly infinite
69 varieties of activity patterns. This flexibility implies that our brains' activity patterns are highly
70 information rich. However, brain activity patterns are also highly structured. For example,
71 full-brain correlation matrices are stable within (Finn et al., 2017, 2015; Gratton et al., 2018) and
72 across (Cole et al., 2014; Glerean et al., 2012; Gratton et al., 2018; Yeo et al., 2011) individuals. This
73 stability suggests that our brains' activity patterns are at least partially constrained, for example
74 by anatomical, external, or internal factors. Constraints on brain activity that limit its flexibility
75 decrease expressiveness (i.e., its information rate). However, constraints on brain activity also
76 increase its robustness to noise (e.g., "missing" or corrupted signals may be partially recovered).
77 For example, recent work has shown that full-brain activity patterns may be reliably recovered
78 from only a relatively small number of implanted electrodes (Owen et al., 2020; Scangos et al.,
79 2021). This robustness property suggests that the relevant signal (e.g., underlying factors that
80 have some influence over brain activity patterns) are compressible.

81 To the extent that brain activity patterns contain rich task-relevant information, we should be
82 able to use the activity patterns to accurately differentiate between different aspects of a task (e.g.,
83 using pattern classifiers; Norman et al., 2006). For example, prior work has shown a direct
84 correspondence between classification accuracy and the information content of a signal (Alvarez,
85 2002). To the extent that brain activity patterns are compressible, we should be able to generate
86 simplified (e.g., lower dimensional) representations of the data while still preserving the relevant
87 or important aspects of the original signal. In general, information content and compressibility
88 are often related but are also dissociable (Fig. 1). If a given signal (e.g., a representation of brain
89 activity patterns) contains more information about ongoing cognitive processes, then the peak
90 decoding accuracy should be high. In the simulations shown in Figure 1C we construct synthetic
91 datasets that have high or low levels of informativeness by varying temporal autocorrelations
92 in the data (see *Synthetic data*). If a signal is compressible, then a low-dimensional embedding
93 of the signal will be similarly informative as the original signal. In the simulations shown in
94 Figure 1C we construct synthetic datasets that have high or low levels of compressibility by
95 varying the covariance structure across features (see *Synthetic data*). As shown in Figure 1D, highly

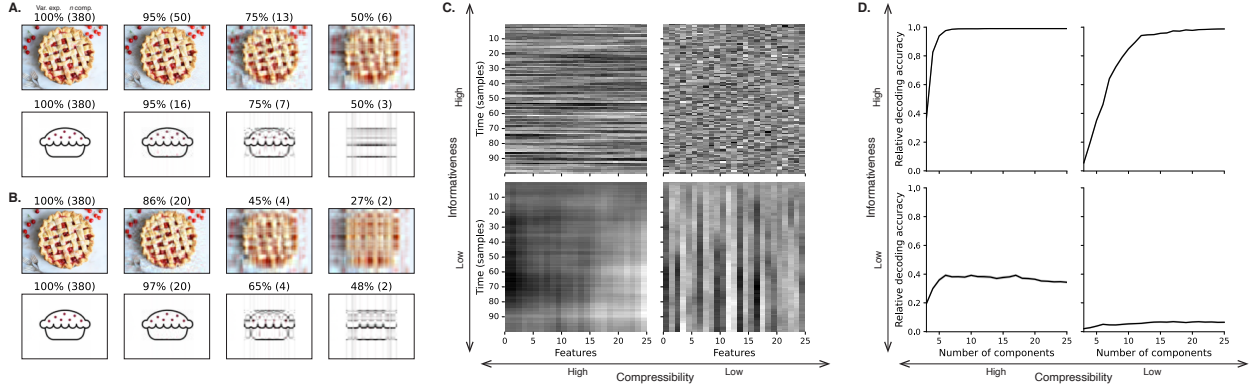


Figure 1: Information content and compressibility. **A. Variance explained for two images.** Consider two example images: a photograph and simple drawing. The images have the same resolutions, but their content is very different. The photograph is more information rich: when we compare the original photograph and drawing (leftmost column), we can see that the photograph captures much more detail. We can also apply principal components analysis to the images, treating the rows of the images as “observations.” Across columns, we identified the numbers of components required to explain 100%, 95%, 75%, or 50% of the cumulative variance in each image (the 100% columns denote the original images). The numbers of components are indicated in parentheses, and the resulting “compressed” images are displayed. This analysis reveals that the drawing is more compressible: just 16 components can explain 95% of the variance in the drawing, whereas 50 components are required to explain 95% of the variance in the photograph. **B. Representing two images with different numbers of components.** Using the same principal component decompositions as in Panel A, we computed the cumulative proportion of variance explained with 380 (original images), 20, 4, or 2 components. This analysis provides another way of characterizing the compressibility of each image by showing that the same number of components can explain more variance in the drawing than in the photograph. **C. Template data from four synthetic datasets.** We constructed four synthetic datasets, each comprising 25 features (columns) observed across 100 samples (rows) from each of 10 simulated “participants.” The datasets were constructed to contain different levels of informativeness and compressibility (see *Synthetic data*). **D. Decoding accuracy by number of components.** For each synthetic dataset, we trained across-participant classifiers to decode timepoint labels. Each panel displays the decoding accuracy as a function of the number of components used to represent the data. Error ribbons denote bootstrap-estimated 95% confidence intervals.

96 informative datasets yield higher decoding accuracies than less informative datasets (i.e., the peaks
97 of the curves in the top panels of Fig. 1D are higher than the peaks of the curves in the bottom
98 panels). Highly compressible datasets show steeper slopes when we plot decoding accuracy as a
99 function of the number of components used to represent the data (i.e., the slopes of the curves in
100 the left panels of Fig. 1D are steeper than the slopes of the curves in the right panels). Whereas
101 characterizing the informativeness and compressibility of synthetic data can be instructive, we
102 are ultimately interested in understanding how these properties relate to brain activity patterns
103 recorded under different cognitive circumstances.

104 Several recent studies suggest that the complexity of brain activity is task-dependent, whereby
105 simpler tasks with lower cognitive demands are reflected by simpler and more compressible brain
106 activity patterns, and more complex tasks with higher cognitive demands are reflected by more
107 complex and less compressible brain activity patterns (Mack et al., 2020; Owen et al., 2021). These
108 findings complement other work suggesting that functional connectivity (correlation) patterns are
109 task-dependent (Cole et al., 2014; Finn et al., 2017; Owen et al., 2020), although see Gratton et
110 al. (2018). Higher-order cognitive processing of a common stimulus also appears to drive more
111 stereotyped task-related activity and functional connectivity across individuals (Hasson et al.,
112 2008; Lerner et al., 2011; Simony & Chang, 2020; Simony et al., 2016).

113 The above studies are consistent with two potential descriptions of how cognitive processes are
114 reflected in brain activity patterns. One possibility is that the information rate of brain activity in-
115 creases during more complex or higher-level cognitive processing. If so, then the ability to reliably
116 decode cognitive states from brain activity patterns should improve with task complexity or with
117 the level (or “depth”) of cognitive processing. A second possibility is that the compressibility of
118 brain activity patterns increases during more complex or higher-level cognitive processing. If so,
119 then individual features of brain recordings, or compressed representations of brain recordings,
120 should carry more information during complex or high-level (versus simple or low-level) cognitive
121 tasks.

122 We used a previously collected neuroimaging dataset to estimate the extent to which each of
123 these two possibilities might hold. The dataset we examined comprised functional magnetic res-
124 onance imaging (fMRI) data collected as participants listened to an audio recording of a 7-minute
125 story, temporally scrambled recordings of the story, or underwent a resting state scan (Simony

126 et al., 2016). Each of these experimental conditions evokes different depths of cognitive process-
127 ing (Hasson et al., 2008; Lerner et al., 2011; Owen et al., 2021; Simony et al., 2016). We used
128 across-participant classifiers to decode listening times in each condition, as a proxy for how “infor-
129 mative” the task-specific activity patterns were (Simony & Chang, 2020). We also used principle
130 components analysis to generate lower-dimensional representations of the activity patterns. We
131 then repeated the classification analyses after preserving different numbers of components and
132 examined how classification accuracy changed across the different experimental conditions.

133 Results

134 We sought to understand whether higher-level cognition is reflected by more reliable and in-
135 formative brain activity patterns, and how compressibility of brain activity patterns relates to
136 cognitive complexity. We developed a computational framework for systematically assessing the
137 informativeness and compressibility of brain activity patterns recorded under different cognitive
138 circumstances. We used across-participant decoding accuracy (see *Forward inference and decoding*
139 *accuracy*) as a proxy for informativeness. To estimate the compressibility of the brain patterns, we
140 used group principal components analysis (PCA) to project the brain patterns into k -dimensional
141 spaces, for different values of k (see *Hierarchical Topographic Factor Analysis (HTFA)* and *Principal*
142 *components analysis (PCA)*). For more compressible brain patterns, decoding accuracy should be
143 more robust to small values of k .

144 We analyzed a dataset collected by Simony et al. (2016) that comprised four experimental con-
145 ditions. These conditions exposed participants to stimuli that systematically varied in cognitive
146 engagement. In the *intact* experimental condition, participants listened to an audio recording of
147 a 7-minute Moth Radio Hour story, *Pie Man*, by Jim O’Grady. In the *paragraph*-scrambled experi-
148 mental condition, participants listened to a temporally scrambled version of the story, where the
149 paragraphs occurred out of order, but where the same set of paragraphs was presented over the
150 entire listening interval. All participants in this condition experienced the scrambled paragraphs
151 in the same order. In the *word*-scrambled experimental condition, participants listened to a tem-
152 porally scrambled version of the story, where the words occurred in a random order. Again, all
153 participants in this condition experienced the scrambled words in the same order. Finally, in the

154 *rest* experimental condition, participants lay in the scanner with no overt stimulus, while keeping
155 their eyes open and blinking as needed. This public dataset provided a convenient means for
156 testing our hypothesis that different levels of cognitive processing and engagement affect how
157 informative and compressible the associated brain patterns are.

158 To evaluate the relation between informativeness and compressibility for brain activity from
159 each experimental condition, we trained a series of across-participant temporal decoders on com-
160 pressed representations of the data. Figure 2A displays the decoding accuracy as a function
161 of the number of principal components used to represent the data (also see Fig. S1). Several
162 patterns were revealed by the analysis. First, in general (i.e., across experimental conditions),
163 decoding accuracy tends to improve as the number of components are increased. However, de-
164 coding accuracy peaked at higher levels for experimental conditions that exposed participants
165 to cognitively richer stimuli (Fig. 2D). The peak decoding accuracy was highest for the “intact”
166 condition (versus paragraph: $t(99) = 35.205, p < 0.001$; versus word: $t(99) = 43.172, p < 0.001$);
167 versus rest: $t(99) = 81.361, p < 0.001$), next highest for the “paragraph” condition (versus word:
168 $t(99) = 6.243, p < 0.001$; versus rest: $t(99) = 50.748, p < 0.001$), and next highest for the “word”
169 condition (versus rest: $t(99) = 48.791, p < 0.001$). This ordering implies that cognitively richer
170 conditions evoke more stable brain activity patterns across people.

171 The cognitively richer conditions also displayed steeper initial slopes. For example, the intact
172 condition decoders reached an arbitrarily chosen threshold of 5% accuracy using fewer components
173 than the paragraph condition decoders ($t(99) = -7.429, p < 0.001$) or word condition decoders
174 ($t(99) = -7.300, p < 0.001$), and decoding accuracy never exceeded 5% for the rest condition. This
175 suggests that brain activity patterns evoked by cognitively richer conditions are more compressible,
176 such that representing the data using the same number of principal components provides more
177 information to the temporal decoders (Figs. 2B, C). Taken together, as shown in Figure 2E, we
178 found that brain activity patterns evoked by cognitively richer conditions tended to be both more
179 informative (i.e., associated with higher peak decoding accuracies) *and* more compressible (i.e.,
180 requiring fewer components to achieve the 5% accuracy threshold).

181 If informativeness (to the temporal decoders) and compressibility vary with the cognitive
182 richness of the stimulus, might these measures also vary over time *within* a given condition? For
183 example, participants in the intact condition might process the ongoing story more deeply later

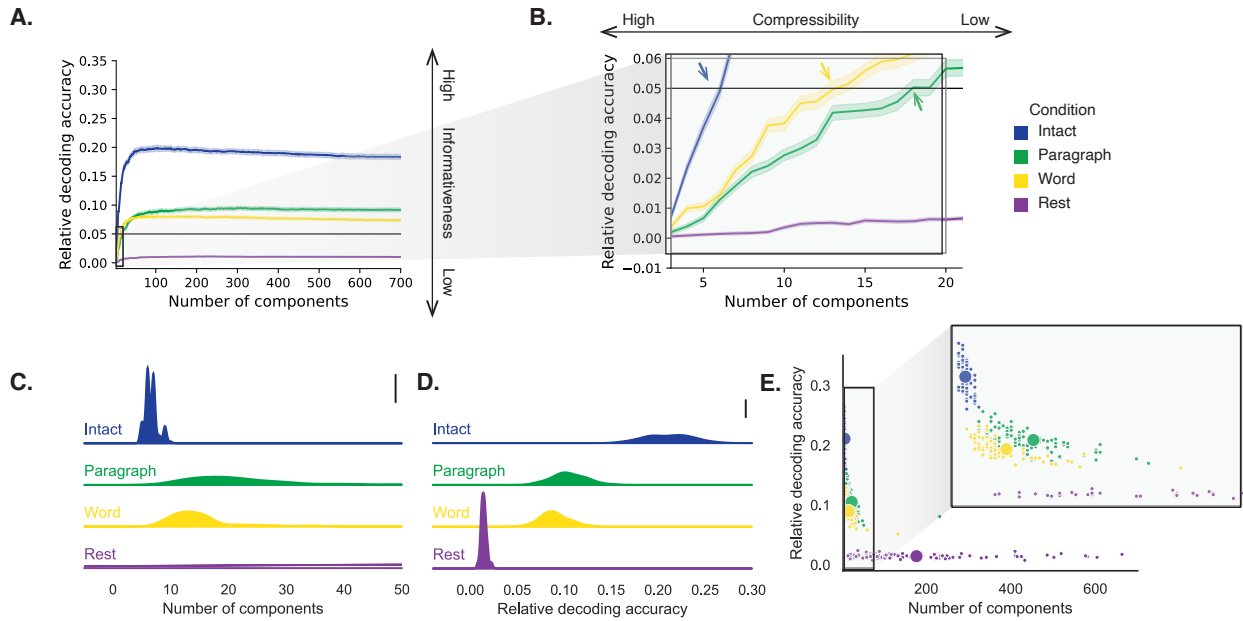


Figure 2: Decoding accuracy and compressibility.

A. Decoding accuracy by number of components. Ribbons of each color display cross-validated decoding performance for each condition (intact, paragraph, word, and rest), as a function of the number of components (features) used to represent the data. For each condition, decoding accuracy has been normalized by subtracting expected “chance” decoding performance (estimated as $\frac{1}{T}$, where T is the number of timepoints in the given condition). This normalization was intended to enable fairer comparisons across conditions; a relative decoding accuracy of 0.0 denotes “chance” performance. The horizontal black line denotes 5% decoding accuracy (used as a reference in Panel B).

B. Numbers of components required to reach a fixed decoding accuracy threshold, by condition. The panel displays a zoomed-in view of the inset in Panel A. Intersections between each condition’s decoding accuracy curve and the 5% decoding accuracy reference line are marked by arrows. All error ribbons in Panels A and B denote bootstrap-estimated 95% confidence intervals.

C. Estimating “compressibility” for each condition. The probability density plots display the numbers of components required to reach at least 5% (corrected) decoding accuracy, across all cross validation runs. For the “rest” condition, where decoding accuracy never reached 5% accuracy, we display the distribution of the numbers of components required to achieve the peak decoding accuracy in each fold. (This distribution is nearly flat, as also illustrated in Panel E.) The scale bar denotes a height of 0.01.

D. Estimating “informativeness” for each condition. The probability density plots display the peak (corrected) decoding accuracies achieved in each condition, across all cross validation runs. The scale bar denotes a height of 0.01.

E. Informativeness versus compressibility. Each dot displays the minimum number of components required to achieve at least 5% corrected decoding accuracy (x -coordinate; for the rest condition the numbers of components are estimated using the peak decoding accuracies as in Panel C) and the peak (corrected) decoding accuracy (y -coordinate). The smaller dots correspond to individual cross validation runs and the larger dots display the averages across runs. The inset displays a zoomed-in view of the indicated region in the main panel.

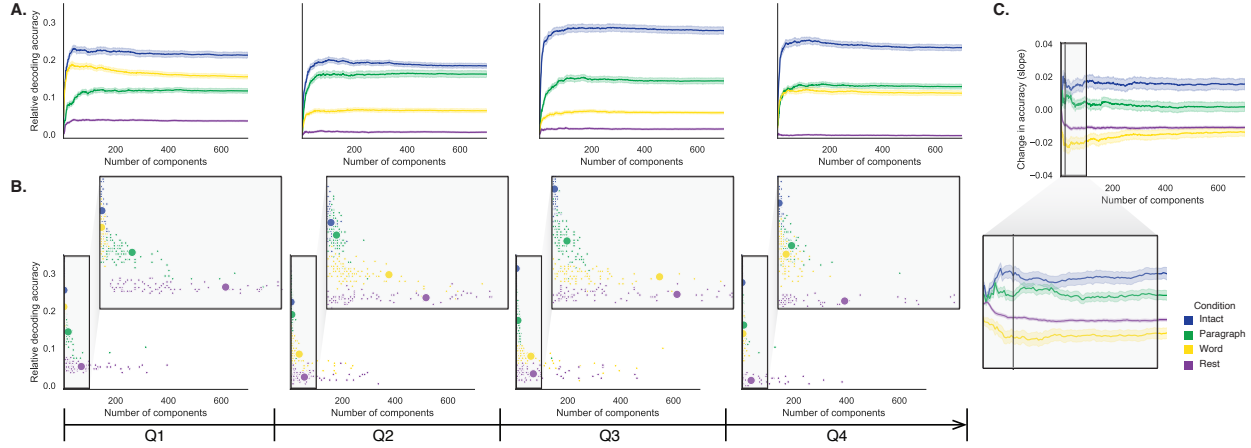


Figure 3: Changes in decoding accuracy and compression over time. **A. Decoding accuracy by number of components, by story segment.** Each family of curves is plotted in the same format as Figure 2A but reflects data only from one quarter of the dataset. **B. Informativeness versus compressibility by condition and segment.** Each scatter plot is in the same format as Figure 2E, but reflects data only from one quarter of the dataset. **C. Change in decoding accuracy over time, by number of components.** For each number of components (x -axis) and condition (color), we fit a regression line to the decoding accuracies obtained for the first, second, third, and fourth quarters of the dataset (corresponding to the columns of Panels A and B). The y -axis denotes the slopes of the regression lines. The black vertical line marks $k = 20$ components, as referenced in the main text. All error ribbons denote bootstrap-estimated 95% confidence intervals.

on in the story (compared with earlier in the story) given the additional narrative background and context they had been exposed to by that point. To examine this possibility, we divided each condition into four successive time segments. We computed decoding curves (Fig. 3A) and the numbers of components required to achieve 5% decoding accuracy (Fig. 3B) for each segment and condition. We found that, in the two most cognitively rich conditions (intact and paragraph), both decoding accuracy and compressibility, as reflected by the change in decoding curves, increased with listening time (e.g., at the annotated reference point of $k = 20$ components in Fig. 3C: intact: $t(99) = 7.915, p < 0.001$; paragraph: $t(99) = 2.354, p = 0.021$). These changes may reflect an increase in comprehension or depth of processing with listening time. In contrast, the decoding accuracy and compressibility decreased with listening time in the word condition ($t(99) = -10.747, p < 0.001$) and rest condition ($t(99) = -22.081, p < 0.001$). This might reflect the depletion of attentional resources in the less-engaging word and rest conditions.

These results make some intuitive sense. As the contextual information available to participants increases (i.e., over time in the cognitively rich intact and paragraph conditions), it makes sense that

198 this might constrain neural responses to a greater extent. While this pattern may not necessarily
199 hold for *every* possible story or stimulus, we suspect that it is generally the case that our knowledge
200 about what is happening in a story tends to increase as we experience more about it. In turn, this
201 could lead to greater consistency in different people's interpretations of and neural responses to
202 the stimulus. Similarly, as participants are left to "mind wander," or as they experience mental
203 fatigue (i.e., over time in the less cognitively rich word and rest conditions), we suggest that this
204 might lead to greater variability in neural responses across people, resulting in lower decoding
205 accuracy. Again, it is not necessarily the case that every possible "unengaging" stimulus will
206 lead to greater neural variability as time progresses, but we suspect this phenomenon is likely to
207 hold for a variety of such stimuli. These findings replicate at least to a limited extent (e.g., across
208 both cognitively rich conditions and across both cognitively impoverished conditions, and for the
209 different groups of participants in each of those conditions). However, determining whether these
210 patterns generalize to other stimuli would require additional study (with new stimuli).

211 If the informativeness and compressibility of brain activity patterns vary over time, do these
212 properties might also vary across brain networks? We used a network parcellation identified by Yeo
213 et al. (2011) to segment the brain into seven distinct networks. The networks can be sorted (roughly)
214 in order from lower-level to higher-level cortex as follows (Figs. 4A–C): visual, somatomotor,
215 dorsal attention, ventral attention, limbic, frontoparietal, and default mode. Next, we computed
216 decoding curves separately for the activity patterns within each network and identified each
217 network's inflection point, for each experimental condition. Moving from low-order networks
218 to higher-order networks, we found that decoding accuracy tended to increase in the higher-
219 level experimental conditions and decrease (slightly) in the lower-level experimental conditions
220 (Fig. 4D, E; Spearman's rank correlation between decoding accuracy and network order: intact:
221 $\rho = 0.362, p < 0.001$; paragraph: $\rho = 0.441, p < 0.001$; word: $\rho = -0.102, p = 0.007$; rest: $\rho =$
222 $-0.354, p < 0.001$). This suggests that higher-order networks may carry more content-relevant
223 or stimulus-driven "information." We found no clear trends in the proportions of components
224 required to achieve 5% decoding accuracy across networks or conditions (Fig. 4F). We note that
225 the limbic network we considered here often overlaps with low (imaging) signal regions, and
226 therefore it may be difficult to draw strong conclusions about this network's informativeness or
227 compressibility.

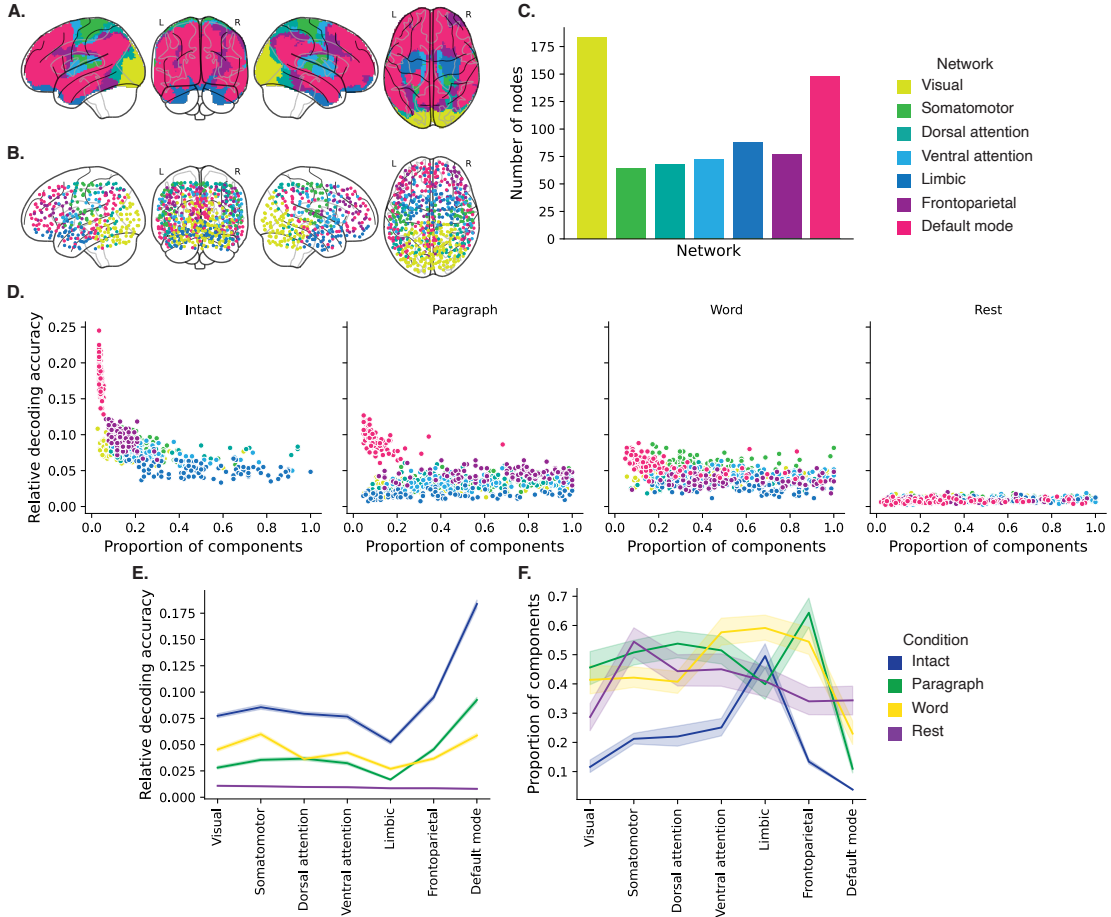


Figure 4: Network-specific decoding accuracy and compression. **A. Network parcellation map.** The glass brain displays the location of each of seven networks identified by Yeo et al. (2011). **B. Node labels.** We assigned network labels to each of 700 Hierarchical Topographic Factor Analysis-derived nodes (see *Hierarchical topographic factor analysis (HTFA)*). For each node, we evaluated its radial basis function (RBF) at the locations of every voxel in the parcellation map displayed in Panel A. We summed up these RBF weights separately for the voxels in each network. We defined each node's network label as its highest-weighted network across all voxels. **C. Per-network node counts.** The bar plot displays the total number of HTFA-derived nodes assigned to each network. **D. Informativeness versus compressibility by network and condition.** Each dot corresponds to a single cross validation run. The dots' coordinates denote the minimum proportion of components (relative to the number of nodes in the given network) required to achieve at least 5% corrected decoding accuracy (x -coordinate; for the rest condition these proportions are estimated using the peak decoding accuracies) and peak (corrected) decoding accuracy (y -coordinate). We repeated the analysis separately for each network (color) and experimental condition (column). **E. Informativeness by network.** For each network, sorted (roughly) from lower-order networks on the left to higher-order networks on the right, the curves display the peak (corrected) decoding accuracy for each experimental condition (color). **F. Compressibility by network.** For each network, the curves display the proportion of components (relative to the total possible number of components displayed in Panel C) required to achieve at least 5% decoding accuracy (or, for the rest condition, peak decoding accuracy, as described above). Error ribbons in Panels E and F denote bootstrap-estimated 95% confidence intervals.

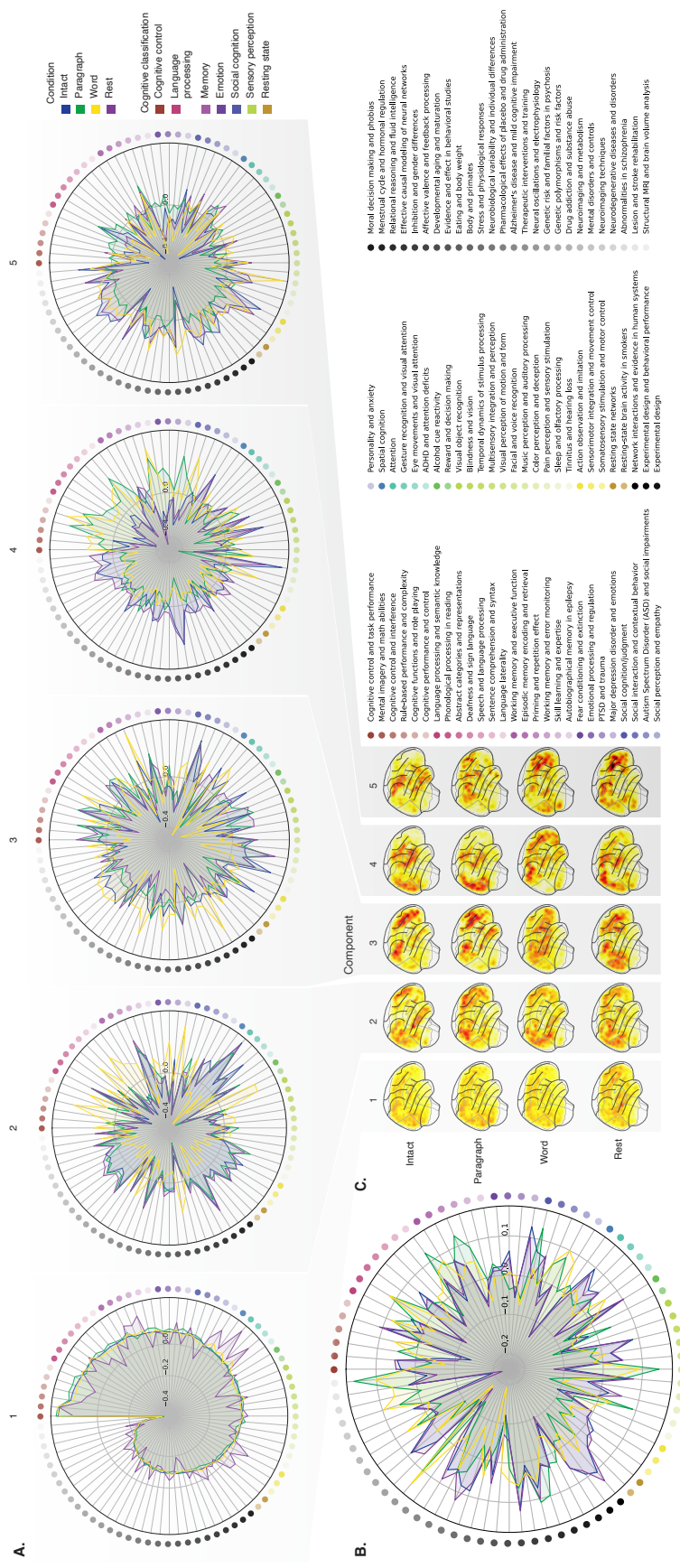


Figure 5: Neurosynth topic weightings by component. We used a reverse inference procedure (see *Reverse inference*) to estimate the correspondences between brain images and a set of 80 topics derived from the Neurosynth database of neuroimaging articles (Rubin et al., 2017). **A. Topic correlations by component.** For each of the top five highest-weighted principal components (columns) derived from each experimental condition (colors), the radar plots display the correlations between the component images and the per-topic images derived for each topic (topic identities are denoted by the blue dots; a legend for the topic labels is in the lower right of the figure). An annotated list of the top-weighted topics for each component and condition may be found in Figure S2 and the top-weighted terms for each topic may be found in Table S1. **B. Topic correlations averaged across components.** The radar plot is in the same format as the plots in Panel A, but here we display the per-condition average correlations across the top five components (for each condition) reflected in Panel A. **C. Component images.** Each plot displays a right sagittal view of a glass brain projection of the top five principal components (columns) for each experimental condition (rows). Additional projections for each component may be found in Figure S3.

228 Whereas the above analyses examine different networks in isolation, how does full-brain
229 (i.e., potentially multi-network) activity patterns reflected by different principal components vary
230 across different experimental conditions? As shown in Figure 5, we used Neurosynth (Rubin et al.,
231 2017) to identify, for each component, the associations with each of 80 themes (see *Reverse inference*).
232 In general, the first principal components across all of the experimental conditions tended to weight
233 most heavily on themes related to cognitive control, memory, language processing, attention, and
234 perception. Other components appeared to vary more across conditions.

235 To gain further insights into which brain functions might be most closely associated with
236 the top-weighted components from each experimental condition, we manually grouped each
237 Neurosynth-derived topic into a smaller set of core cognitive functions. Separately for each com-
238 ponent, we computed the average weightings across all topics that were tagged as being associated
239 with each of these cognitive functions (Figs. 6A, S5A). To help visualize these associations, we used
240 the patterns of associations for each component to construct graphs whose nodes were experimen-
241 tal conditions and cognitive functions (Figs. 6B, S5B). We also computed correlations between the
242 sets of per-topic weightings from each of the top-weighted components from each experimental
243 condition (Fig. 6C, D) and between the brain maps for each condition's components (Fig. S5C, D).
244 Taken together, we found that each component appeared to weight on a fundamental set of cogni-
245 tive functions that varied by experimental condition. For example, the top principal components
246 from every condition weighted similarly (across conditions) on the full set of Neurosynth topics
247 (Fig. 5A) and cognitive functions (Figs. 6A, B and S5 A, B), suggesting that these components might
248 reflect a set of functions or activity patterns that are common across all conditions. The second
249 components' weightings were similar across the intact, paragraph, and rest conditions (highest-
250 weighted functions: cognitive control, memory, social cognition, and resting state), but different
251 for the word condition (highest-weighted functions: sensory perception and cognitive control).
252 The fourth components' weighting grouped the paragraph and word conditions (highest-weighted
253 functions: memory, language processing, and cognitive control) and the intact and rest conditions
254 (highest-weighted functions: emotion, social cognition). We also used ChatGPT (OpenAI, 2023)
255 to sort the list of manually tagged cognitive functions from lowest-level to highest-level (Tab. S2,
256 Fig. 6E; also see *Ranking cognitive processes*). We found that higher-level functions tended to be
257 weighted on more heavily by top components from the intact and paragraph conditions than lower-

258 level functions (intact vs. word: $t(198) = 11.059, p < 0.001$; intact vs. rest: $t(198) = 3.699, p < 0.001$;
259 paragraph vs. word: $t(198) = 13.504, p < 0.001$; paragraph vs. rest: $t(198) = 4.812, p < 0.001$; also
260 see *Ranking cognitive processes*). The top components from the word condition showed the opposite
261 tendency, whereby *lower*-level functions tended to be weighted on more heavily than higher-level
262 functions (word vs. rest: $t(198) = -7.315, p < 0.001$). The weighting trends for the intact and
263 paragraph conditions were not reliably different ($t(198) = -0.479, p = 0.633$). The components
264 from the rest condition showed almost no differences in the weights associated with high-level
265 versus low-level functions (rest vs. 0: $t(99) = 1.836, p = 0.081$). These findings suggest that when
266 participants were engaged more strongly (in the more engaging intact and paragraph conditions),
267 their dominant neural patterns reflected higher-level cognitive functions. In contrast, when partic-
268 ipants were engaged less strongly (in the less engaging word and rest conditions), their dominant
269 neural patterns reflected lower-level cognitive functions. Although they were highly statistically
270 reliable, it is also important to note that these latter effects are also relatively small (e.g., the slopes
271 for *all* of the experimental conditions are numerically close to zero; Fig. 6E). We suggest that this
272 phenomenon may merit further investigation in future work.

273 Discussion

274 We examined fMRI data collected as participants listened to an auditory recording of a story, scram-
275 bled recordings of the story, or underwent a resting state scan. We found that cognitively richer
276 stimuli evoked more reliable (i.e., consistent across people) and information rich brain activity pat-
277 terns. The brain patterns evoked by cognitively richer stimuli were also more compressible, in that
278 each individual component provided more “signal” to temporal decoders relative to components
279 of data from less cognitively rich conditions (Fig. 2). Over time (e.g., as the experiment progressed),
280 these phenomena were strengthened. Specifically, across story segments, data from more cogni-
281 tively rich conditions became more informative and compressible, and data from less cognitively
282 rich conditions became *less* informative and compressible (Fig. 3). We also repeated these analyses
283 separately for different brain networks. We found that networks traditionally associated with
284 higher-level cognitive functions tended to provide more informative brain patterns than networks
285 traditionally associated with lower level cognitive functions (Fig. 4). Finally, we examined the most

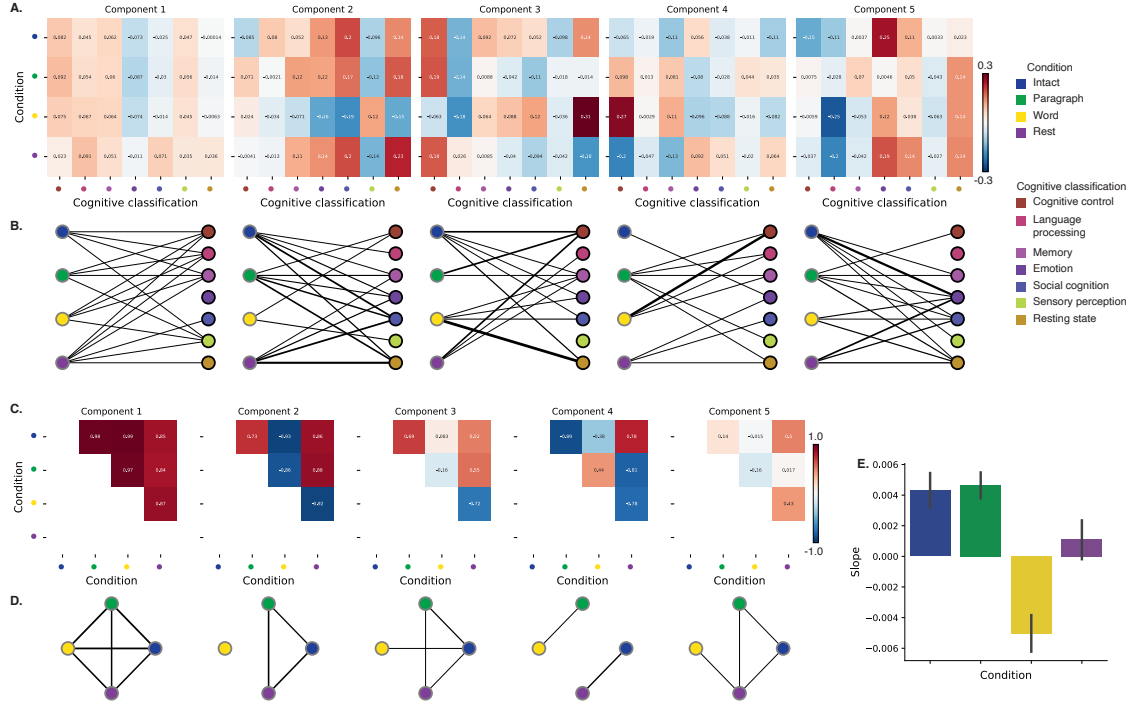


Figure 6: Summary of functions associated with top-weighted components by condition. A. Top-weighted topics by condition. Here we display per-condition (rows, indicated by colored dots) topic correlations, averaged across topics that pertain to each of several broad cognitive functions (columns within each sub-panel, indicated by colored dots). Each sub-panel reflects correlations for the components indicated in the panel titles. A legend for the condition and several core cognitive function classifications is displayed in the lower right of the figure. Table S1 provides a list of each topic's top-weighted terms, along with each topic's manually labeled cognitive classification. A full list of the topics most highly associated with each component may be found in Figure S2. **B. Associations between per-condition components and cognitive functions.** The network plots denote positive average correlations between the component images for each condition (gray-outlined dots on the left sides of each network; colors denote conditions) and topic-specific brain maps associated with each indicated cognitive function (black-outlined dots on the right sides of each network; colors denote cognitive functions). The line thicknesses are proportional to the correlation values (correlation coefficients are noted in the heat maps in Panel A). **C. Correlations between each principal component, by condition.** The heat maps display the correlations between the brain maps (Fig. S3) for each principal component (sub-panel), across each pair of conditions (rows and columns of each sub-panel's matrix, indicated by colored dots). **D. Associations between per-condition components, by component.** Each sub-panel's network plot summarizes the pattern of correlations between the n^{th} top-weighted principal components (sub-panel) for each experimental condition (gray-outlined dots). The line thicknesses are proportional to the correlation values (correlation coefficients are noted in the heat maps in Panel C). **E. Change in weights by condition.** The bar heights reflect the slopes of regression lines, fit separately to the top five components from each condition, between the ChatGPT-derived “rank” of each cognitive classification and the correlations between the component and topic maps associated with cognitive processes at the given rank (see *Ranking cognitive processes*) Error bars denote bootstrap-estimated 95% confidence intervals. Also see Fig. S5 for additional information.

286 dominant components of the brain activity patterns from each experimental condition. We used a
287 reverse inference approach (Rubin et al., 2017) to identify the terms in the neuroimaging literature
288 most commonly associated with the corresponding maps. As summarized in Figure 6E, we found
289 that the intact and paragraph conditions tended to weight on higher-level cognitive processes
290 more than lower-level cognitive processes, whereas the word condition weighted on lower-level
291 processes more than higher-level processes and the rest condition showed no difference in high-
292 level versus low-level weighting. Taken together, our findings indicate that the informativeness
293 and compressibility of our brain activity patterns are task-dependent, and these properties change
294 systematically with factors like cognitive richness and depth of processing.

295 Our explorations of informativeness and compressibility are related to a much broader litera-
296 ture on the correlational and causal structure of brain activity patterns and networks (Adachi et
297 al., 2012; Bassett & Sporns, 2017; Brovelli et al., 2004; Bullmore & Sporns, 2009; Dhamala et al.,
298 2008; Korzeniewska et al., 2008; Lynn & Bassett, 2021; Owen et al., 2021; Preti et al., 2017; Rogers
299 et al., 2007; Rubinov & Sporns, 2010; Sizemore et al., 2018; Smith, Beckmann, et al., 2013; Smith,
300 Vidaurre, et al., 2013; Sporns & Betzel, 2016; Sporns & Honey, 2006; Sporns & Zwi, 2004; Srinivasan
301 et al., 2007; Tomasi & Volkow, 2011; Yeo et al., 2011). Correlations or causal associations between
302 different brain regions simultaneously imply that full-brain activity patterns will be compressible
303 and also that those activity patterns will contain redundancies. For example, the extent to which
304 activity patterns at one brain area can be inferred or predicted from activity patterns at other
305 areas (e.g., Owen et al., 2020; Scangos et al., 2021), reflects overlap in the information available
306 in or represented by those brain areas. If brain patterns in one area are recoverable using brain
307 patterns in another area, then a “signal” used to convey the activity patterns could be compressed
308 by removing the recoverable activity. Predictable (and therefore redundant) brain activity patterns
309 are also more robust to signal corruption. For example, even if the activity patterns at one region
310 are unreadable or unreliable at a given moment, that unreliability could be compensated for by
311 other regions’ activity patterns that were predictive of the unreliable region. Whereas compress-
312 ible brain patterns are robust to spatial signal corruption, high versus low informativeness reflects
313 a similar (though dissociable; e.g., Fig. 1) tradeoff between expressiveness and robustness of *tem-*
314 *poral* patterns. Highly informative brain patterns (by our measure; i.e., patterns that yield greater
315 temporal decoding accuracy) are expressive about ongoing experiences or cognitive states, since

316 each moment's pattern is reliably distinguishable from other moments' patterns. However, when
317 each moment's pattern is unique, brain activity becomes less robust to temporal signal corruption.
318 Our finding that brain activity patterns becomes more informative (i.e., less robust to temporal
319 signal corruption) and compressible (i.e., more robust to spatial signal corruption) when cognitive
320 engagement is higher suggests that our brain may optimize its activity patterns to prioritize either
321 temporal or spatial robustness, according to task demands.

322 Our findings that informativeness and compressibility change with task demands may follow
323 from task-dependent changes in full-brain correlation patterns. A number of prior studies have
324 found that so-called "functional connectivity" (i.e., correlational) patterns vary reliably across
325 tasks, events, and situations (Cole et al., 2014; Owen et al., 2021; Simony et al., 2016; Smith et
326 al., 2009). By examining how these task-dependent changes in correlations affect informativeness
327 and compressibility, our work suggests a potential reason why the statistical structure of brain
328 activity patterns might vary with cognitive task or with cognitive demands. For lower-level tasks,
329 or for tasks that require relatively little "deep" cognitive processing, our brains may optimize
330 activity patterns for robustness and redundancy over expressiveness, for example to maximize
331 reliability. For higher-level tasks, or for tasks that require deeper cognitive processing, our brains
332 may sacrifice some redundancy in favor of greater expressiveness.

333 In the information theory sense (Shannon, 1948), when a signal is transmitted using a fixed
334 alphabet of "symbols," the information rate decreases as the signal is compressed (e.g., fewer sym-
335 bols transmitted per unit time, using an alphabet with fewer symbols, etc.). Our finding that each
336 individual brain component (symbol) becomes more informative as cognitive richness increases
337 suggests that the "alphabet" of brain activity patterns is also task-dependent. Other work suggests
338 that the representations that are *reflected* by brain activity patterns may also change with task de-
339 mands. For example, our brains may represent the same perceptual stimulus differently depending
340 on which aspects of the stimulus or which combinations of features are task-relevant (Mack et al.,
341 2020).

342 We found that different brain networks varied in how informative and compressible their
343 activity patterns were across experimental conditions (e.g., Fig. 4). This might follow from evolu-
344 tionary optimizations that reflect the relevant constraints or demands placed on those networks.
345 One possibility is that cortex is organized in a hierarchy of networks "concerned with" or selective

346 to different levels of processing or function. To the extent that different levels of processing (e.g.,
347 low-level sensory processing versus “deeper” higher-level processing) reflect different stimulus
348 timescales (e.g., Manning, 2020), the network differences we observed might also relate to the
349 timescales at which each network is maximally sensitive (Baldassano et al., 2017; Hasson et al.,
350 2008; Lerner et al., 2011; Regev et al., 2018).

351 Our reverse inference analyses (Figs. 5, 6) also provide some insights into how neural activity
352 patterns change with cognitive engagement or task demands. Prior work has shown that the
353 components and network “parcels” identified through covarying activity patterns can be highly
354 similar even across different tasks (including “rest,” e.g., Laird et al., 2011; Smith et al., 2009).
355 We replicated this basic finding in that the first principal components from all four experimental
356 conditions were strikingly similar (e.g., see the leftmost columns of Figs. 5A and 6C, D). We also
357 found some small, though statistically reliable, systematic changes in the weights associated with
358 different cognitive functions across conditions (Fig. 6E). This result provided an additional way of
359 characterizing network-level differences across conditions (Fig. 4E). Taken together, these findings
360 suggest that although similar networks may be involved in different tasks, the ways in which those
361 networks are engaged may vary systematically with task demands.

362 **Concluding remarks**

363 Cognitive neuroscientists are still grappling with basic questions about the fundamental “rules”
364 describing how our brains respond, and about how brain activity patterns and the associated
365 underlying cognitive representations and computations are linked. We identified two aspects of
366 brain activity patterns, informativeness and compressibility, that appear to change systematically
367 with task demands and across brain networks. We speculate that these changes may reflect ongoing
368 tradeoffs between how robust to signal corruption versus how expressive about ongoing cognitive
369 states our brains’ activity patterns are. Our work also provides a new framework for evaluating
370 these tradeoffs in other datasets, or in future studies.

371 **Methods**

372 We measured properties of recorded neuroimaging data under different task conditions that varied
373 systematically in cognitive engagement and depth of processing. We were especially interested in
374 how *informative* and *compressible* the activity patterns were under these different conditions (Fig. 1).

375 Unless otherwise noted, all statistical tests are two-sided, all error bars and error ribbons
376 denote bootstrap-estimated 95% confidence intervals across participants, and all reported *p*-values
377 are corrected for multiple comparisons using the Benjamini-Hochberg procedure (Benjamini &
378 Hochberg, 1995).

379 **Functional neuroimaging data collected during story listening**

380 We examined an fMRI dataset collected by Simony et al. (2016) that the authors have made publicly
381 available at arks.princeton.edu/ark:/88435/dsp015d86p269k. The dataset comprises neuroimaging
382 data collected as participants listened to an audio recording of a story (intact condition; 36 par-
383 ticipants), listened to temporally scrambled recordings of the same story (17 participants in the
384 paragraph-scrambled condition listened to the paragraphs in a randomized order and 36 in the
385 word-scrambled condition listened to the words in a randomized order), or lay resting with their
386 eyes open in the scanner (rest condition; 36 participants). Full neuroimaging details may be found
387 in the original paper for which the data were collected (Simony et al., 2016). Procedures were
388 approved by the Princeton University Committee on Activities Involving Human Subjects, and by
389 the Western Institutional Review Board (Puyallup, WA). All subjects were native English speakers
390 with normal hearing and provided written informed consent. We have excerpted the relevant
391 portions of the dataset documentation here to provide information about the scanning parameters
392 and preprocessing steps used to generate the data we analyzed (the original descriptions may be
393 found at the above link):

394 Subjects were scanned in a 3T full-body MRI scanner (Skyra; Siemens) with a sixteen-
395 channel head coil. For functional scans, images were acquired using a T2* weighted
396 echo planer imaging (EPI) pulse sequence [repetition time (TR), 1500 ms; echo time (TE),
397 28 ms; flip angle, 64°], each volume comprising 27 slices of 4 mm thickness with 0 mm
398 gap; slice acquisition order was interleaved. In-plane resolution was 3 × 3 mm² [field of

view (FOV), $192 \times 192 \text{ mm}^2$]. Anatomical images were acquired using a T1-weighted magnetization-prepared rapid-acquisition gradient echo (MPRAGE) pulse sequence (TR, 2300 ms; TE, 3.08 ms; flip angle 9°; 0.89 mm^3 resolution; FOV, 256 mm 2). To minimize head movement, subjects' heads were stabilized with foam padding. Stimuli were presented using the Psychophysics toolbox (Brainard, 1997; Pelli, 1997). Subjects were provided with an MRI compatible in-ear mono earbuds (Sensimetrics Model S14), which provided the same audio input to each ear. MRI-safe passive noise-canceling headphones were placed over the earbuds, for noise removal and safety.

Functional data were preprocessed and analyzed using FSL (www.fmrib.ox.ac.uk/fsl), including correction for head motion and slice-acquisition time, spatial smoothing (6 mm FWHM Gaussian kernel), and high-pass temporal filtering (140 s period). Preprocessed data were aligned to coplanar and high-resolution anatomicals and the standard MNI152 brain, and interpolated to 3-mm isotropic voxels.

The intact and word conditions each comprised 300 TRs (7.5 minutes) per participant. The paragraph condition comprised 272 TRs (6.8 minutes) per participant. The rest condition comprised 400 TRs (10 minutes) per participant.

Hierarchical topographic factor analysis (HTFA)

Following our prior related work, we used HTFA (Manning et al., 2018) to derive a compact representation of the neuroimaging data. In brief, this approach approximates the timeseries of voxel activations (44,415 voxels) using a much smaller number of radial basis function (RBF) nodes (in this case, 700 nodes, as determined by an optimization procedure; Manning et al., 2018). This provides a convenient representation for examining full-brain activity patterns and network dynamics. All of the analyses we carried out on the neuroimaging dataset were performed in this lower-dimensional space. In other words, each participant's data matrix was a number-of-timepoints (T) by 700 matrix of HTFA-derived factor weights (where the row and column labels were matched across participants). Code for carrying out HTFA on fMRI data may be found as part of the BrainIAK toolbox (Capota et al., 2017; Kumar et al., 2021), which may be downloaded at brainiak.org.

427 We also considered alternative approaches to obtaining compact representations of the neu-
428 roimaging data, including network parcellations (e.g., Gordon et al., 2016; Schaefer et al., 2018).
429 Whereas network parcellations are typically derived from large resting state datasets, HTFA may
430 be applied to much smaller datasets. In our prior work, we showed that HTFA applied to the same
431 dataset used here can explain full-brain activity to within a maximum of 0.25 standard deviations
432 of each voxel’s observed activity in the original dataset, taken across all voxels, images, and par-
433 ticipants, using the 700-node representation we also employed here (Manning et al., 2018). Some
434 of the explanatory power of HTFA comes from the fact that each node’s explanatory power falls
435 off smoothly with distance to its center. Intuitively, the result is a representation that looks like a
436 lightly spatially smoothed version of the original data, but where the degree of smoothing varies
437 across the brain according to how spatially autocorrelated the local activity patterns are.

438 **Principal components analysis (PCA)**

439 We applied group PCA (Smith et al., 2014) separately to the HTFA-derived representations of the
440 data (i.e., factor loadings) from each experimental condition. Specifically, for each condition, we
441 considered the set of all participants’ T by 700 factor weight matrices. We used group PCA to project
442 these 700-dimensional matrices into a series of shared k -dimensional spaces, for $k \in \{3, 4, 5, \dots, 700\}$.
443 This yielded a set of number-of-participants matrices, each with T rows and k columns.

444 **Temporal decoding**

445 We sought to identify neural patterns that reflected participants’ ongoing cognitive processing of
446 incoming stimulus information. As reviewed by Simony et al. (2016), one way of homing in on
447 these stimulus-driven neural patterns is to compare activity patterns across individuals. In partic-
448 ular, neural patterns will be similar across individuals to the extent that the neural patterns under
449 consideration are stimulus-driven, and to the extent that the corresponding cognitive representa-
450 tions are reflected in similar spatial patterns across people (Simony & Chang, 2020). Following this
451 logic, we used an across-participant temporal decoding test developed by Manning et al. (2018) to
452 assess the degree to which different neural patterns reflected ongoing stimulus-driven cognitive
453 processing across people. The approach entails using a subset of the data to train a classifier to

454 decode stimulus timepoints (i.e., moments in the story participants listened to) from neural pat-
455 terns. We use decoding (forward inference) accuracy on held-out data, from held-out participants,
456 as a proxy for the extent to which the inputted neural patterns reflected stimulus-driven cognitive
457 processing in a similar way across individuals.

458 **Forward inference and decoding accuracy**

459 We used an across-participant correlation-based classifier to decode which stimulus timepoint
460 matched each timepoint’s neural pattern. For a given value of k (i.e., number of principal compo-
461 nents), we first used group PCA to project the data from each condition into a shared k -dimensional
462 space. Next, we divided the participants into two groups: a template group, $\mathcal{G}_{\text{template}}$ (i.e., training
463 data), and a to-be-decoded group, $\mathcal{G}_{\text{decode}}$ (i.e., test data). We averaged the projected data within
464 each group to obtain a single T by k matrix for each group. Next, we correlated the rows of the two
465 averaged matrices to form a T by T decoding matrix, Λ . In this way, the rows of Λ reflected time-
466 points from the template group, while the columns reflected timepoints from the to-be-decoded
467 group. We used Λ to assign temporal labels to each timepoint (row) from the test group’s ma-
468 trix, using the row of the training group’s matrix with which it was most highly correlated. We
469 repeated this decoding procedure, but using $\mathcal{G}_{\text{decode}}$ as the template group and $\mathcal{G}_{\text{template}}$ as the
470 to-be-decoded group. Given the true timepoint labels (for each group), we defined the decoding
471 accuracy as the average proportion of correctly decoded timepoints, across both groups (where
472 chance performance is $\frac{1}{T}$). In Figures 2 and 3 we report the decoding accuracy for each condition
473 and value of k , averaged across $n = 100$ cross validation folds.

474 **Reverse inference**

475 To help interpret the brain activity patterns we found within the contexts of other studies, we
476 created summary maps of each principal component, for each experimental condition. Each
477 principal component comprises 700 “weights” on each of the HTFA-derived RBF nodes (see
478 *Hierarchical Topographic Factor Analysis*). For each node, we evaluated its RBF at the locations of
479 every voxel in the standard 2 mm MNI152 template brain and multiplied the RBF by the node’s
480 weight. The sum of these weighted RBF activation maps provides a full-brain image, in MNI152

481 space, of the given principal component (Fig. S3).

482 Next, we considered 80 topics estimated using Latent Dirichlet Allocation (Blei et al., 2003)
483 applied to 9,204 functional neuroimaging articles in the Neurosynth database (Rubin et al., 2017).
484 The topics, as well as associated brain maps identified using Neurosynth, were identified and
485 reported in several prior studies (Chen et al., 2020; Fox et al., 2014; Sul et al., 2017). The topic
486 labels for each topic were generated automatically with the following ChatGPT (OpenAI, 2023)
487 prompt: “Please help me come up with intuitive labels for topics I found by fitting a topic model
488 to thousands of neuroscience and psychology articles. I’ll paste in the top 10 highest-weighted
489 words for each topic, and I’d like you to respond with a suggested label. For each topic, please
490 respond with just the topic label and no other formatting or text. Here are the next topic’s top
491 words:” followed by a comma-separated list of the given topic’s top-weighted words reflected
492 in the Table S1. For some topics, ChatGPT responded with a longer-form response rather than a
493 concise topic label. In these instances, on a case-by-case basis, we used a second follow-up prompt
494 to achieve the given topic’s label: “Could you please come up with a more concise label for that
495 topic?”. We then manually identified a set of 11 cognitive labels that were intended to encapsulate
496 a representative range of widely studied low-level and high-level cognitive functions. In choosing
497 the set of cognitive labels, we jointly considered each topic’s ChatGPT-derived topic label, along
498 with the top-weighted words for the topic. We attempted to generate a concise set of labels that
499 still spanned the full set of cognitive functions reflected across the 80 topics. Topics that appeared
500 unrelated to specific cognitive functions (e.g., topics related to specific methods or clinical themes)
501 are designated with dashes in Table S1.

502 Finally, following an approach used in several prior studies (Chen et al., 2020; Fox et al., 2014;
503 Sul et al., 2017) we treated the correlation between a given component’s brain map and each topic’s
504 brain map as an approximate measure of how much the component was reflective of the given
505 topic. This resulted in a set of 80 “weights” (correlation coefficients) for each component’s brain
506 map, with one weight per Neurosynth-derived topic.

507 **Ranking cognitive processes**

508 We manually identified 11 cognitive labels spanning the set of 80 Neurosynth-derived topics:
509 cognitive control, language processing, memory, emotion, social cognition, spatial cognition, at-
510 tention, reward, sensory perception, motor control, and resting state. We then used ChatGPT
511 to automatically “rank” the processes from high-level to low-level using the following prompt:
512 “Please rank these cognitive processes from highest-level to lowest-level, where higher values
513 indicate higher-order or higher-level processes. Return the result as a csv file with a header row
514 and two columns: ‘Cognitive label’ and ‘Rank’. Here are the processes: cognitive control, lan-
515 guage processing, memory, emotion, social cognition, spatial cognition, attention, reward, sensory
516 perception, motor control, resting state”. Table S2 displays the output.

517 We recognize that ChatGPT is not omniscient, nor should it be treated as an expert cognitive
518 neuroscientist. We therefore reviewed ChatGPT’s responses carefully by hand to verify that they
519 seemed reasonable to us. Whereas prior work has often constructed such rankings by hand, we see
520 our use of ChatGPT in this case as a small additional “sanity check” on our rankings that helped
521 us to be slightly more objective than if we had simply created the rankings ourselves manually.

522 In the analysis presented in Figure 6E, we summarize difference in topic weightings across
523 experimental conditions. In particular, we sought to characterize how the dominant neural patterns
524 evoked by each experimental condition weighted on different cognitive functions. For each of the
525 top five principal components from each experimental condition (Fig. 5), we computed the average
526 weightings for each of the 11 manually identified (and ChatGPT-ranked) cognitive labels described
527 above (Tab. S2). We then fit a line separately for each experiment condition (x -values: cognitive
528 rank; y -values: weights). In carrying out this analysis, we used a bootstrap procedure to estimate
529 the variability in the slopes of the regression lines, whereby we repeated this process for each of
530 $n = 100$ iterations, each time resampling (with replacement) the set of observed ranks and weights.
531 This procedure yielded distributions of 100 estimated slopes for each experimental condition. We
532 used these distributions to compare the slopes across experimental conditions and to estimate 95%
533 confidence intervals.

534 **Synthetic data**

535 To help illustrate the relationship between informativeness and compressibility (Fig. 1), we gen-
536 erated four synthetic datasets, varying in informativeness and compressibility. Each dataset com-
537 prised simulated observations of $K = 25$ features across $N = 100$ timepoints, from each of $S = 10$
538 participants. To create each dataset, we first constructed a “template” matrix of N timepoints by K
539 features. We then generated participant-specific data by adding independent noise to each entry
540 in template matrix, drawn from the unit normal distribution (i.e., with a mean of 0 and a variance
541 of 1). We repeated this process for each participant, yielding S participant-specific matrices for
542 each dataset.

543 Since we estimate informativeness using the temporal decoding accuracy across participants,
544 highly informative data will tend to have observations that are highly timepoint specific. Relatively
545 uninformative data, in contrast, will tend to have more similar observations across timepoints. To
546 generate data with “high informativeness,” we constructed template matrices whose rows (ob-
547 servations) were drawn independently from zero-mean multivariate normal distributions. The
548 covariances of these distributions were determined according to the desired compressibility of
549 the data, as described below. We used a multi-step process to generate data with “low informa-
550 tiveness.” First we generated new template matrices using the same procedure as for the “high
551 informativeness” datasets. We then multiplied each matrix by a constant ($\rho = 0.1$) and computed
552 the cumulative sum of each matrix’s rows. This yielded matrices whose rows were highly similar
553 across observations.

554 Compressibility reflects the extent to which decoding accuracy is affected by reducing the num-
555 ber of components used to represent the data. Highly compressible data will tend to exhibit more
556 similarities across features, whereas less compressible data will tend to show greater independence
557 across features. To generate data with “high compressibility,” we set the covariance matrix of the
558 multivariate normal distribution to a toeplitz matrix whose first row was given by $[K, K - 1, \dots, 1]$.
559 To generate data with “low compressibility,” we set the covariance matrix to the identity matrix.

560 Template matrices for datasets with high informativeness and high compressibility, high in-
561 formative and low compressibility, low informativeness and high compressibility, and low
562 informativeness and low compressibility are displayed in Figure 1C. The corresponding decoding

563 curves are displayed in Figure 1D.

564 Data and code availability

565 All of the code used to produce the figures and results in this manuscript, along with links to the
566 corresponding data, may be found at github.com/ContextLab/pca_paper.

567 Acknowledgements

568 We acknowledge discussions with Rick Betzel, Luke Chang, Emily Finn, and Jim Haxby. Our
569 work was supported in part by NSF CAREER Award Number 2145172 to J.R.M. The content is
570 solely the responsibility of the authors and does not necessarily represent the official views of our
571 supporting organizations. The funders had no role in study design, data collection and analysis,
572 decision to publish, or preparation of the manuscript.

573 Author contributions

574 Conceptualization: J.R.M. and L.L.W.O. Methodology: J.R.M. and L.L.W.O. Implementation:
575 J.R.M. and L.L.W.O. Analysis: J.R.M. and L.L.W.O. Writing, Reviewing, and Editing: J.R.M. and
576 L.L.W.O. Funding acquisition: J.R.M. Supervision: J.R.M.

577 References

578 Adachi, Y., Osada, T., Sporns, O., Watanabe, T., Matsui, T., Miyamoto, K., & Miyashita, Y.
579 (2012). Functional connectivity between anatomically unconnected areas is shaped by collective
580 network-level effects in the macaque cortex. *Cerebral Cortex*, 22(7), 1586–1592.

581 Alvarez, S. A. (2002). *An exact analytical relation among recall, precision, and classification accuracy in*
582 *information retrieval* (Technical Report No. BCCS-02-01). Boston College.

583 Baldassano, C., Chen, J., Zadbood, A., Pillow, J. W., Hasson, U., & Norman, K. A. (2017). Discov-
584 ering event structure in continuous narrative perception and memory. *Neuron*, 95(3), 709–721.

- 585 Bassett, D. S., & Sporns, O. (2017). Network neuroscience. *Nature Neuroscience*, 20(3), 353–364.
- 586 Benjamini, Y., & Hochberg, Y. (1995). Controlling the False Discovery Rate: a practical and
587 powerful approach to multiple testing. *Journal of Royal Statistical Society, Series B*, 57, 289–300.
- 588 Blei, D. M., Ng, A. Y., & Jordan, M. I. (2003). Latent dirichlet allocation. *Journal of Machine Learning
589 Research*, 3, 993–1022.
- 590 Brainard, D. H. (1997). The psychophysics toolbox. *Spatial Vision*, 10, 443–446.
- 591 Brovelli, A., Ding, M., Ledberg, A., Chen, Y., Nakamura, R., & Bressler, S. (2004). Beta oscillations in
592 a large-scale sensorimotor cortical network: directional influences revealed by Granger causality.
593 *Proceedings of the National Academy of Sciences, USA*, 101(26), 9849–9854.
- 594 Bullmore, E., & Sporns, O. (2009). Complex brain networks: graph theoretical analysis of structural
595 and functional systems. *Nature Reviews Neuroscience*, 10(3), 186–198.
- 596 Capota, M., Turek, J., Chen, P.-H., Zhu, X., Manning, J. R., Sundaram, N., ... Shin, Y. S. (2017).
597 *Brain imaging analysis kit*.
- 598 Chen, P.-H. A., Jolly, E., Cheong, J. H., & Chang, L. J. (2020). Intersubject representational
599 similarity analysis reveals individual variations in affective experience when watching erotic
600 movies. *NeuroImage*, 216(116851), doi.org/10.1016/j.neuroimage.2020.116851.
- 601 Cole, M. W., Bassett, D. S., Power, J. D., Braver, T. S., & Petersen, S. E. (2014). Intrinsic and
602 task-evoked network architectures of the human brain. *Neuron*, 83(1), 238–251.
- 603 Dhamala, M., Rangarajan, G., & Ding, M. (2008). Analyzing information flow in brain networks
604 with nonparametric Granger causality. *NeuroImage*, 41(2), 354–362.
- 605 Finn, E. S., Scheinost, D., Finn, D. M., Shen, X., Papademetris, X., & Constable, R. T. (2017).
606 Can brain state be manipulated to emphasize individual differences in functional connectivity.
607 *NeuroImage*, 160, 140–151.
- 608 Finn, E. S., Shen, X., Scheinost, D., Rosenberg, M. D., Huang, J., Chun, M. M., ... Constable, R. T.
609 (2015). Functional connectome fingerprinting: identifying individuals using patterns of brain
610 connectivity. *Nature Neuroscience*, 18, 1664–1671.

- 611 Fox, A. S., Chang, L. J., Gorgolewski, K. J., & Yarkoni, T. (2014). Bridging psychology and
612 genetics using large-scale spatial analysis of neuroimaging and neurogenetic data. *bioRxiv*,
613 doi.org/10.1101/012310.
- 614 Glerean, E., Salmi, J., Lahnakoski, J. M., Jääskeläinen, I. P., & Sams, M. (2012). Functional magnetic
615 resonance imaging phase synchronization as a measure of dynamic functional connectivity.
616 *Brain Connectivity*, 2(2), 91–101.
- 617 Gordon, E. M., Laumann, T. O., Adeyemo, B., Huckins, J. F., Kelley, W. M., & Petersen, S. E. (2016).
618 Generation and evaluation of a cortical area parcellation from resting-state correlations. *Cerebral
619 Cortex*, 26, 288–303.
- 620 Gratton, C., Laumann, T. O., Nielsen, A. N., Greene, D. J., Gordon, E. M., Gilmore, A. W., ...
621 Petersen, S. E. (2018). Functional brain networks are dominated by stable group and individual
622 factors, not cognitive or daily variation. *Neuron*, 98(2), 439–452.
- 623 Hasson, U., Yang, E., Vallines, I., Heeger, D. J., & Rubin, N. (2008). A hierarchy of temporal
624 receptive windows in human cortex. *The Journal of Neuroscience*, 28(10), 2539–2550.
- 625 Korzeniewska, A., Crainiceanu, C. M., Kus, R., Franaszczuk, P. J., & Crone, N. E. (2008). Dynamics
626 of event-related causality in brain electrical activity. *Human Brain Mapping*, 29(10).
- 627 Kumar, M., Anderson, M. J., Antony, J. W., Baldassano, C., Brooks, P. P., Cai, M. B., ... Norman,
628 K. A. (2021). BrainIAK: the brain image analysis kit. *Aperture*, doi.org/10.52294/31bb5b68-2184-
629 411b-8c00-a1dacb61e1da.
- 630 Laird, A. R., Fox, P. M., Eickhoff, S. B., Turner, J. A., Ray, K. L., McKay, D. R., ... Fox, P. T. (2011).
631 Behavioral interpretations of intrinsic connectivity networks. *Journal of Cognitive Neuroscience*,
632 23(12), 4022–4037.
- 633 Lerner, Y., Honey, C. J., Silbert, L. J., & Hasson, U. (2011). Topographic mapping of a hierarchy of
634 temporal receptive windows using a narrated story. *The Journal of Neuroscience*, 31(8), 2906–2915.
- 635 Lynn, C. W., & Bassett, D. S. (2021). Quantifying the compressibility of complex networks.
636 *Proceedings of the National Academy of Sciences, USA*, 118(32), e2023473118.

- 637 Mack, M. L., Preston, A. R., & Love, B. C. (2020). Ventromedial prefrontal cortex compressesion
638 during concept learning. *Nature Communications*, 11(46), doi.org/10.1038/s41467-019-13930-8.
- 639 Manning, J. R. (2020). Context reinstatement. In M. J. Kahana & A. D. Wagner (Eds.), *Handbook of*
640 *human memory*. Oxford University Press.
- 641 Manning, J. R., Zhu, X., Willke, T. L., Ranganath, R., Stachenfeld, K., Hasson, U., ... Norman,
642 K. A. (2018). A probabilistic approach to discovering dynamic full-brain functional connectivity
643 patterns. *NeuroImage*, 180, 243–252.
- 644 Norman, K. A., Polyn, S. M., Detre, G. J., & Haxby, J. V. (2006). Beyond mind-reading: multi-voxel
645 pattern analysis of fMRI data. *Trends in Cognitive Sciences*, 10(9), 424–430.
- 646 OpenAI. (2023). *ChatGPT*. <https://chat.openai.com>.
- 647 Owen, L. L. W., Chang, T. H., & Manning, J. R. (2021). High-level cognition during story listening is
648 reflected in high-order dynamic correlations in neural activity patterns. *Nature Communications*,
649 12(5728), doi.org/10.1038/s41467-021-25876-x.
- 650 Owen, L. L. W., Muntianu, T. A., Heusser, A. C., Daly, P., Scangos, K. W., & Manning, J. R. (2020). A
651 Gaussian process model of human electrocorticographic data. *Cerebral Cortex*, 30(10), 5333–5345.
- 652 Pelli, D. G. (1997). The VideoToolbox software for visual psychophysics: transforming numbers
653 into movies. *Spatial Vision*, 10, 437–442.
- 654 Preti, M. G., Bolton, T. A. W., & Van De Ville, D. (2017). The dynamic functional connectome:
655 state-of-the-art and perspectives. *NeuroImage*, 160, 41–54.
- 656 Regev, M., Simony, E., Lee, K., Tan, K. M., Chen, J., & Hasson, U. (2018). Propagation of information
657 along the cortical hierarchy as a function of attention while reading and listening to stories.
658 *Cerebral Cortex*.
- 659 Rogers, B. P., Morgan, V. L., Newton, A. T., & Gore, J. C. (2007). Assessing functional connectivity
660 in the human brain by fMRI. *Magnetic Resonance Imaging*, 25(11), 1347–1357.

- 661 Rubin, T. N., Kyojo, O., Gorgolewski, K. J., Jones, M. N., Poldrack, R. A., & Yarkoni, T. (2017).
662 Decoding brain activity using a large-scale probabilistic functional-anatomical atlas of human
663 cognition. *PLoS Computational Biology*, 13(10), e1005649.
- 664 Rubinov, M., & Sporns, O. (2010). Complex network measures of brain connectivity: uses and
665 interpretations. *NeuroImage*, 52, 1059–1069.
- 666 Scangos, K. W., Khambhati, A. N., Daly, P. M., Owen, L. L. W., Manning, J. R., Ambrose, J. B.,
667 ... Chang, E. F. (2021). Biomarkers of depression symptoms defined by direct intracranial
668 neurophysiology. *Frontiers in Human Neuroscience*, 15, doi.org/10.3389/fnhum.2021.746499.
- 669 Schaefer, A., Kong, R., Gordon, E. M., Laumann, T. O., Z, X.-N., Holmes, A. J., ... Yeo, B. T. T. (2018).
670 Local-global parcellation of the human cerebral cortex from intrinsic functional connectivity MRI.
671 *Cerebral Cortex*, 28, 3095–3114.
- 672 Shannon, C. E. (1948). A mathematical theory of communication. *Bell System Technical Journal*,
673 27(3), 379–423.
- 674 Simony, E., & Chang, C. (2020). Analysis of stimulus-induced brain dynamics during naturalistic
675 paradigms. *NeuroImage*, 216, 116461.
- 676 Simony, E., Honey, C. J., Chen, J., & Hasson, U. (2016). Dynamic reconfiguration of the default
677 mode network during narrative comprehension. *Nature Communications*, 7(12141), 1–13.
- 678 Sizemore, A. E., Giusti, C., Kahn, A., Vettel, J. M., Betzel, R. F., & Bassett, D. S. (2018). Cliques and
679 cavities in the human connectome. *Journal of Computational Neuroscience*, 44(1), 115–145.
- 680 Smith, S. M., Beckmann, C. F., Andersson, J., Auerbach, E. J., Bijsterbosch, J., Douaud, G., ...
681 Glasser, M. F. (2013). Resting-state fMRI in the Human Connectome Project. *NeuroImage*, 80,
682 144–168.
- 683 Smith, S. M., Fox, P. T., Miller, K. L., Glahn, D. C., Fox, P. M., Mackay, C. E., ... Beckmann,
684 C. F. (2009). Correspondence of the brain's functional architecture during activation and rest.
685 *Proceedings of the National Academy of Sciences, USA*, 106(31), 13040–13045.

- 686 Smith, S. M., Hyvärinen, A., Varoquaux, G., Miller, K. L., & Beckmann, C. F. (2014). Group-PCA
687 for very large fMRI datasets. *NeuroImage*, 101, 738–749.
- 688 Smith, S. M., Vidaurre, D., Beckmann, C. F., Glasser, M. F., Jenkinson, M., Miller, K. L., . . . Van
689 Essen, D. C. (2013). Functional connectomics from resting-state fMRI. *Trends in Cognitive Sciences*,
690 17(12), 666–682.
- 691 Sporns, O., & Betzel, R. F. (2016). Modular brain networks. *Annual Review of Psychology*, 67,
692 613–640.
- 693 Sporns, O., & Honey, C. J. (2006). Small worlds inside big brains. *Proceedings of the National Academy
of Sciences, USA*, 103(51), 19219–19220.
- 694
- 695 Sporns, O., & Zwi, J. D. (2004). The small world of the cerebral cortex. *Neuroinformatics*, 2(2),
696 145–162.
- 697 Srinivasan, R., Winter, W. R., Ding, J., & Nunez, P. L. (2007). EEG and MEG coherence: Measures of
698 functional connectivity at distinct spatial scales of neocortical dynamics. *Journal of Neuroscience
Methods*, 166, 41–52.
- 699
- 700 Sul, S., Güroğlu, B., Crone, E. A., & Chang, L. J. (2017). Medial prefrontal cortical thinning
701 mediates shifts in other-regarding preferences during adolescence. *Scientific Reports*, 7(8510),
702 doi.org/10.1038/s41598-017-08692-6.
- 703 Tomasi, D., & Volkow, N. D. (2011). Association between functional connectivity hubs and brain
704 networks. *Cerebral Cortex*, 21, 2003–2013.
- 705 Yeo, B. T. T., Krienen, F. M., Sepulcre, J., Sabuncu, M. R., Lashkari, D., Hollinshead, M., . . . Buckner,
706 R. L. (2011). The organization of the human cerebral cortex estimated by intrinsic functional
707 connectivity. *Journal of Neurophysiology*, 106(3), 1125–1165.